Journal of Materials Chemistry C

RSC Publishing

PAPER

View Article Online
View Journal | View Issue

Cite this: J. Mater. Chem. C, 2013, 1, 2886

Polyaniline stabilized barium titanate nanoparticles reinforced epoxy nanocomposites with high dielectric permittivity and reduced flammability†

Xi Zhang,[ab] Qingliang He,[ab] Hongbo Gu,[ab] Suying Wei*[b] and Zhanhu Guo*[a]

Epoxy polymer nanocomposites (PNCs) filled with both barium titanate ($BaTiO_3$) (500 and 100 nm) and conductive polyaniline (PANI) stabilized $BaTiO_3$ nanoparticles (NPs) have been successfully prepared. The effects of the $BaTiO_3$ nanofiller loading level and the PANI coating on the mechanical properties, rheological behavior, thermal stability, flammability and dielectric properties were systematically studied. The viscosity study on the nanosuspensions indicates that the PANI layer on the $BaTiO_3$ nanoparticle surface can promote the network formation of the epoxy resin. The introduction of the PANI layer was found to reduce the heat release rate and to increase the char residue of the epoxy resin. The dynamic storage and loss moduli were studied together with the glass transition temperature (T_g) obtained from the peak of tan δ, and the reduced T_g in the PNCs is associated with the enlarged free volume. The tensile test indicated an improved tensile strength of the epoxy matrix with the introduction of the $BaTiO_3$ NPs. Compared with the cured pure epoxy, the elasticity modulus was increased for all the PNC samples. The fracture surface study revealed an enhanced toughness. Due to the ferroelectric nature of $BaTiO_3$, the real dielectric permittivity increased with increasing the $BaTiO_3$ nanoparticle loading. The PANI layer on the surface of $BaTiO_3$ also enhanced the dielectric permittivity arising from the interfacial polarization formed in the PNCs.

Received 21st January 2013
Accepted 26th February 2013

DOI: 10.1039/c3tc30129j

www.rsc.org/MaterialsC

1 Introduction

Polymer nanocomposites (PNCs) are an most important material for the 21st century owing to their potential wide applications arising from the unique nanofiller-introduced thermal stability,[1] electrochemical, mechanical, magnetic and dielectric properties[2–4] compared with the otherwise inert polymers. Epoxy as one of the most important engineering polymers can be used as structural components, and different nanofillers have been applied to obtain multifunctional PNCs. For instance, carbon nanofiber–epoxy resin has been fabricated to obtain enhanced tensile strength and electrical conductivity,[5] and magnetic epoxy has been prepared with Fe_3O_4 nanoparticles (NPs).[6] Recently, materials with high dielectric constant have attracted more interest due to their outstanding property-related performances, such as high energy density, which ensures their potential applications in modern electronics and electrical systems.[7] Barium titanate ($BaTiO_3$) exhibiting unique ferroelectricity,[8] piezoelectricity[9] and high dielectric constant[10] has been used to improve the dielectric properties of various polymers. For example, polyvinylidene fluoride (PVDF) or siloxane-modified polyamideimide (SPAI) filled with $BaTiO_3$ has been used to prepare high dielectric thin films,[11] and nanosized $BaTiO_3$ dispersed in polyvinylpyrrolidone (PVP) and quaternary acrylic resin (RMX) can be applied as high capacitance films[12] and humidity sensors,[13] respectively. The $BaTiO_3$–polystyrene-*block*-poly(styrene-*co*-vinylbenzylchloride) (PS-*b*-PSVBC) core–shell NPs, prepared by dispersing PS-*b*-PSVBC and $BaTiO_3$ NPs in tetrahydrofuran for better dispersibility in the nonpolar polymer matrix, have been used for preparing high-energy density nanocomposites.[14]

Although epoxy–$BaTiO_3$ nanocomposites have outstanding dielectric properties, the utilization of epoxy PNCs is limited by the easy flammability of the epoxy resin.[15] Generally, two types of NPs are applied to enhance the flame retardancy of the polymer matrix. One type consists of inorganic NPs including alumina trihydrate,[16] layered double hydroxides (LDHs),[17] clay[18] and montmorillonite (MMT).[19] During combustion, inorganic nanofillers can enhance the char formation[20] and limit the volatilization of materials produced by the polymer matrix decomposition.[21,22] However, the flame retardancy of the nanocomposites with inorganic NPs largely depends on their dispersion.[16] Due to the poor compatibility between organic and inorganic materials, additional surface modification[23] or

[a]Integrated Composites Laboratory (ICL) Dan F Smith Department of Chemical Engineering, Lamar University, Beaumont, TX 77710, USA. E-mail: zhanhu.guo@lamar.edu; Tel: +1-409-880-7654

[b]Department of Chemistry and Biochemistry, Lamar University, Beaumont, TX 77710, USA. E-mail: suying.wei@lamar.edu; Tel: +1-409-880-7976

† Electronic supplementary information (ESI) available. See DOI: 10.1039/c3tc30129j

compatibilization[24] is required to achieve good dispersion. For instance, organo-modified LDHs were applied to enhance the flame retardancy of epoxy.[20] The other kind of flame retardant nanofillers is organic NPs, such as phosphorus-[25] and nitrogen-based flame retardants.[26] During the research of nanocomposite flame retardancy, nitrogen- based flame retardants have attracted more and more interest due to their efficient performance in all stages of the burning process[26] by releasing ammonia gas[27] and enhancing the char formation.[19]

Polyaniline (PANI), among all the conjugated polymers, is very attractive owing to its controllable doping levels[28–30] and wide range of applications such as in anticorrosion coating,[31] sensors,[32] redox removal of highly toxic Cr(VI) to less toxic and stable Cr(III) from polluted water,[33,34] tissue engineering[35] and electrochemical energy storage cells.[36–38] $BaTiO_3$–PANI PNCs, combining the unique dielectric $BaTiO_3$ and conductive PANI together, have shown great applications. For example, for $BaTiO_3$–PANI composites prepared by mixing $BaTiO_3$ powders with PANI through mechanical grinding, the permittivity at microwave frequency is largely decreased (from 120 to 40) by adding just 5.0 wt% PANI.[39] In addition, $BaTiO_3$–PANI nanocomposites synthesized by *in situ* polymerization with mechanical stirring, can be used as electrorheological (ER) materials. For example, at 3.5 kV mm^{-1} the shear stress of $BaTiO_3$–PANI (20 vol %) in silicone oil can reach 2800 Pa, which is higher than those of pure PANI and pure $BaTiO_3$ in silicone oil.[40] However, the dielectric properties and flammability reduction of epoxy nanocomposites with $BaTiO_3$–PANI particulate nanocomposites as functional nanofillers have not been reported yet.

In this paper, two sizes of $BaTiO_3$ (500 and 100 nm) NPs and lab-synthesized PANI-coated $BaTiO_3$ NPs were applied as nanofillers in epoxy resin to enhance the dielectric properties and to reduce the flammability of the hosting epoxy matrix. PNCs with different kinds and loading levels of nanofillers were prepared. The rheological behaviors of the uncured samples (liquid phase), including viscosity at steady state, complex viscosity and viscosity storage and loss moduli, were studied. For the cured samples (solid phase), the thermal stability was studied by TGA tests and the flammability performance was evaluated by microscale combustion calorimetry considering the heat release capacity (HR capacity), peak heat release rate (pHRR), total heat release, and the char residue. The mechanical properties including tensile strength and Young's modulus and the thermomechanical properties including storage and loss moduli and glass transition temperature were evaluated. The effects of nanofillers and the PANI coating on the dielectric permittivity of the nanocomposites were systematically studied and the observed enhanced dielectric properties were interpreted from the ferroelectric nature of $BaTiO_3$ and the interfacial polarization phenomenon.

2 Experimental

2.1 Materials

The epoxy resin used, Epon 862 (bisphenol F epoxy), and EpiCure W curing agent were purchased from Miller-Stephenson Chemical Company, Inc. Barium titanate ($BaTiO_3$) (500 and 100 nm) NPs were purchased from Nanostructure & Amorphous Materials Inc. Aniline (C_6H_7N, 99.9%), ammonium persulfate (APS, $(NH_4)_2S_2O_8$, reagent grade, 98%) and *p*-toluenesulfonic acid (PTSA, $C_7H_8O_3S$) were all purchased from Sigma Aldrich. Chloroform ($CHCl_3$) was purchased from Fisher Scientific. All the chemicals were used as received without any further treatment.

Preparation of polyaniline-coated $BaTiO_3$ nanocomposite particles. The polyaniline-coated $BaTiO_3$ (500 nm) NPs with a $BaTiO_3$ particle loading of 35.0 wt% were prepared as follows. The molar ratio used was aniline : APS : PTSA = 6 : 3 : 5.[41] For solution one, PTSA (60 mmol), APS (36 mmol) and $BaTiO_3$ NPs (500 nm) were dissolved in deionized water (400 mL), which was then put in an ice-water bath and under ultrasonication for one hour. Solution two was aniline (72 mmol) dissolved in deionized water (100 mL). Then solution two was added into solution one, which was sonicated for an additional one hour in an ice-water bath for polymerization. Finally, the product was vacuum filtered and washed with ethanol and deionized water to remove excess acid, any possible oligomers and organic solvent. Then the obtained powders were dried completely at 50 °C. The PANI would not be able to cover the whole surface of $BaTiO_3$ NPs if the nanoparticle loading was higher than 35.0 wt%. The PANI coating on the small $BaTiO_3$ (100 nm) NPs was observed to be not so good as that on the big $BaTiO_3$ (500 nm) NPs for the same PANI loading. Bare $BaTiO_3$ without PANI coating was observed in the SEM image of $BaTiO_3$ (100 nm)–PANI PNCs even at 1.0 wt% loading of $BaTiO_3$ NPs. To prevent other effects, only PANI-coated $BaTiO_3$ NPs (500 nm) were selected for the subsequent epoxy nanocomposite preparation.

Preparation of epoxy resin nanosuspensions and cured epoxy nanocomposites. The epoxy resin nanosuspensions with 1.0, 5.0, 8.0 and 10.0 wt% $BaTiO_3$ NPs (500 and 100 nm) were prepared as follows. Firstly the $BaTiO_3$ NPs were immersed in epoxy resin (the total weight of epoxy resin and curing agent was fixed to be 40.0 g and the $BaTiO_3$ nanoparticle loading was controlled by varying the weight of the $BaTiO_3$ NPs) without any disturbance overnight so that the resin could wet the nanostructures completely. The mixture was then mechanically stirred (Heidolph, RZR 2041) at a speed of 600 rpm for one hour at room temperature. The curing agent W was added into the above suspension with a weight ratio of monomer/curing agent = 100/26.5 as recommended by the company and the solution was stirred at high speed (600 rpm) for another one hour at room temperature. In order to remove bubbles in the solution and to prevent the precipitation of the $BaTiO_3$ NPs during the curing process, low-speed (200 rpm) mechanical stirring was conducted at 70 °C for 3–4 hours in a water bath. Finally, the solution was poured into silicon rubber molds and cured at 120 °C for 5 hours and then cooled naturally to room temperature.

In addition, to further study the influence of PANI coating, the samples of epoxy resin nanocomposites with 10.0 wt% pure PANI, 28.57 wt% $BaTiO_3$–PANI (contains 10 wt% $BaTiO_3$ and 18.57 wt% PANI) and 15.38 wt% $BaTiO_3$–PANI (contains 5.38 wt% $BaTiO_3$ and 10 wt% PANI) were also prepared.

2.2 Characterization

Rheological behavior of liquid epoxy resin nanosuspensions. The rheological behaviors of the prepared epoxy nanocomposite suspensions were investigated with a rheometer (AR 2000ex, TA Instrumental Company) at shear rates ranging from 0.1 to 1000 s^{-1} at 25 °C. A series of measurements were performed in a cone-and-plate geometry with a diameter of 40 mm and a truncation of 64 μm. Dynamic rheological measurements were also performed with a sweeping frequency range between 0.1 and 100 rad s^{-1} at a low strain (1%), which was justified to be within the linear viscoelastic (LVE) range for these materials. The LVE range was determined by the strain-storage modulus (G') curve within the strain range from 0.01 to 100% at a frequency of 1 rad s^{-1}. Specimens placed between the cone and plate were allowed to equilibrate for approximately two minutes prior to each frequency sweeping.

Thermal characterization of the cured epoxy nanocomposites. The thermal stability of the cured epoxy nanocomposites was studied by thermogravimetric analysis (TGA, Q-500, TA instruments). All the samples were heated from 30 to 700 °C at a nitrogen flow rate of 60 mL min^{-1} and a heating rate of 10 °C min^{-1}. The samples were tested in air at the same flow rate and heating rate to compare the thermal stability of the nanocomposites in different conditions. Differential scanning calorimeter (DSC, TA Instruments Q2000) measurements were implemented under a nitrogen flow rate of approximately 20 mL min^{-1} at a heating rate of 10 °C min^{-1} from 0 to 400 °C.

Flammability of cured epoxy nanocomposites. The flammability performance was evaluated by using a micro-scale combustion calorimeter (MCC, model "MCC-2", Govmark, Farmingdale, New York) according to American Society for Testing and Materials (ASTM D7309 – Method A: Standard Test Method for Determining Flammability Characteristics of Plastics and Other Solid Materials Using Microscale Combustion Calorimetry). The sample (~3 mg) was heated to a specified temperature using a linear heating rate (1 °C s^{-1}) in a stream of nitrogen with a flow rate of 80 mL min^{-1}. The thermal degradation products of the sample in nitrogen were mixed with a 20 mL min^{-1} stream of oxygen prior to entering the 900 °C combustion furnace. The reported MCC parameters were the averages of three measurements.

Mechanical tests of cured epoxy nanocomposites. The dynamic mechanical analysis (DMA) measurements were carried out in the torsion rectangular mode using an AR 2000ex (TA Instrumental Company) with a strain of 0.05%, a constant frequency of 1 Hz and a heating rate of 2 °C min^{-1} in the temperature range of 30–200 °C. The sample dimensions were $12 \times 3 \times 40$ mm^3. The tensile tests were carried out following ASTM (Standard D 412-98a, 2002) in a unidirectional tensile testing machine (ADMET tensile strength testing system). The parameters (displacement and load) were controlled by a digital controller (MTESTQuattro) with MTESTQuattro Materials Testing Software. The samples were prepared as described for the nanocomposite fabrication in silicon rubber molds, which were designed according to the standard ASTM requirement. A crosshead speed of 1.00 mm min^{-1} was used and the strain (mm mm^{-1}) was calculated by dividing the crosshead displacement by the original gauge length.

Morphological characterization of cured nanocomposites. After the tensile test, the broken samples were collected and the morphology of the fracture surfaces was characterized with a field emission scanning electron microscope (SEM, JEOL JSM-6700F). Before testing, the samples were first coated with a thin gold layer.

Permittivity measurements of cured nanocomposites. The dielectric permittivity was measured by a LCR meter (Agilent, E 4980A) equipped with a dielectric test fixture (Agilent, 16451B) at the frequency of 20 to 2×10^6 Hz. The samples used for the tests were disc pellets with a diameter of 40 mm and an average thickness of about 2 mm. A piece of standard rectangular Teflon sample with a permittivity of 2.1–2.4 was used for calibration before each test.

3 Results and discussion

3.1 Rheological behaviors of the liquid epoxy resin nanosuspensions

The rheology behaviors were studied for liquid epoxy resin and its nanosuspensions. For the samples with different loadings and sizes of $BaTiO_3$ NPs, the observed linear relationship between shear rate and shear stress, Fig. 1(A), indicates that the nanosuspension is a Newtonian fluid. However, for the nanosuspensions with $BaTiO_3$–PANI and PANI NPs, Fig. 1(B), the relationship between shear stress and shear rate is no longer linear, and the slope of the curve becomes gentle with increasing the shear rate. The power law model is employed to correlate the shear stress and the shear rate, eqn (1):[42]

$$\sigma = K \times \gamma^n \quad (1)$$

where σ is shear stress, K is consistency, γ is shear rate, and n is the flow behavior index. For a Newtonian fluid, n is equal to one and $n < 1$ for a pseudoplastic fluid. The values of n are summarized in Table 1. For pure liquid epoxy resin ($n = 0.9708$) and the epoxy resin nanosuspension with 10.0 wt% $BaTiO_3$ NPs ($n = 0.9726$), n is almost equal to 1, demonstrating that these two fluids are Newtonian fluids. However, for the epoxy resin nanosuspensions with 10.0 wt% PANI ($n = 0.8693$), 15.38 wt% $BaTiO_3$ (500 nm)–PANI (contains 5.38 wt% $BaTiO_3$ and 10.0 wt% PANI) ($n = 0.8701$) and 28.57 wt% $BaTiO_3$ (500 nm)–PANI (contains 10 wt% $BaTiO_3$ and 18.57 wt% PANI) ($n = 0.7493$), the values of n are all less than one, indicating that these fluids are pseudoplastic fluids. To identify which component of the NPs can lead to the reduction of n, the n values of the nanosuspensions with $BaTiO_3$ (500 nm)–PANI NPs, pure PANI and pure $BaTiO_3$ (500 nm) NPs are compared with each other. For the nanosuspension with 15.38 wt% $BaTiO_3$ (500 nm)–PANI (contains 5.38 wt% $BaTiO_3$ and 10 wt% PANI) and the nanosuspension with 10 wt% PANI, which have the same PANI loading, the n values of both nanosuspensions are almost the same, showing that the $BaTiO_3$ NPs have a negligible effect on the pseudoplastic behavior of the nanosuspensions. However, for the nanosuspensions with 28.57 wt% $BaTiO_3$ (500 nm)–PANI

(contains 10 wt% $BaTiO_3$ and 18.57 wt% PANI) and 10 wt% $BaTiO_3$ (500 nm) NPs, which have the same $BaTiO_3$ nanoparticle loading, the *n* values are completely different. Thus, the *n* value of nanosuspensions with $BaTiO_3$–PANI NPs is determined by the PANI coating on the surface of $BaTiO_3$ NPs. The study of the flow behavior index shows obviously that the PANI coating layer has some reaction with epoxy resins in the nanosuspension with 28.57 wt% $BaTiO_3$ (500 nm)–PANI (contains 10 wt% $BaTiO_3$ and 18.57 wt% PANI) and leads to the transition of the nanosuspensions from Newtonian fluids to pseudoplastic fluids.

Fig. 1(C) and (D) show the viscosity as a function of shear rate. For epoxy nanosuspensions with pure $BaTiO_3$ NPs, Fig. 1(C), a reduced viscosity is observed, the viscosities of nanosuspensions with both big $BaTiO_3$ (1.0, 5.0 wt%) and small $BaTiO_3$ (1.0, 5.0 and 10.0 wt%) NPs are even lower than that of pure epoxy in the whole tested shear rate range. For certain nanosuspensions, NPs with circular shape[43] and a good dispersion were reported to decrease the nanocomposite viscosity.[44] The decreased viscosity is attributed to the dilution effect of NPs, which provides constraint release and leads to viscosity reduction.[43] It is worth noticing that with increasing the loading of $BaTiO_3$ NPs, the viscosity of the nanosuspension with big $BaTiO_3$ NPs (500 nm) increases, which is due to the nanoparticle agglomeration.[44] However, the viscosity of nanosuspension with small $BaTiO_3$ NPs (100 nm) is further decreased and the lowest viscosity is observed in the nanosuspension with 10 wt% $BaTiO_3$ NPs (100 nm), the opposite variation of viscosity with the loading of big and small $BaTiO_3$ NPs indicates that the dilution effect is associated with the nanoparticle size.

In addition, decreased viscosity with increasing shear rate is also observed in the nanosuspensions with pure $BaTiO_3$ NPs. However, due to the justified Newtonian fluid of pure epoxy resin and its nanosuspensions with different loadings of $BaTiO_3$ NPs, the decreased viscosity is only due to the sample splashing under high rotating speed of cone.[45] The Carreau model is employed to correlate the viscosity and the shear rate of the epoxy resin nanosuspensions with 10.0 wt% $BaTiO_3$, 10.0 wt% PANI, 15.38 wt% $BaTiO_3$ (500 nm)–PANI (contains 5.38 wt% $BaTiO_3$ and 10.0 wt% PANI) and 28.57 wt% $BaTiO_3$ (500 nm)–PANI (contains 10 wt% $BaTiO_3$ and 18.57 wt% PANI), eqn (2):[46]

$$\eta = \eta_\infty + \frac{\eta_0 - \eta_\infty}{\left(1 + (C\gamma)^2\right)^{d/2}} \quad (2)$$

where η_∞ is the infinite shear viscosity (limiting viscosity at infinite shear rate, $\eta_\infty = \lim_{\gamma \to \infty} \eta$), η_0 is the zero shear viscosity (limiting viscosity at zero shear rate,[47] $\eta_0 = \lim_{\gamma \to 0} \eta$), *C* is the cross time constant, which represents the transition to a constant

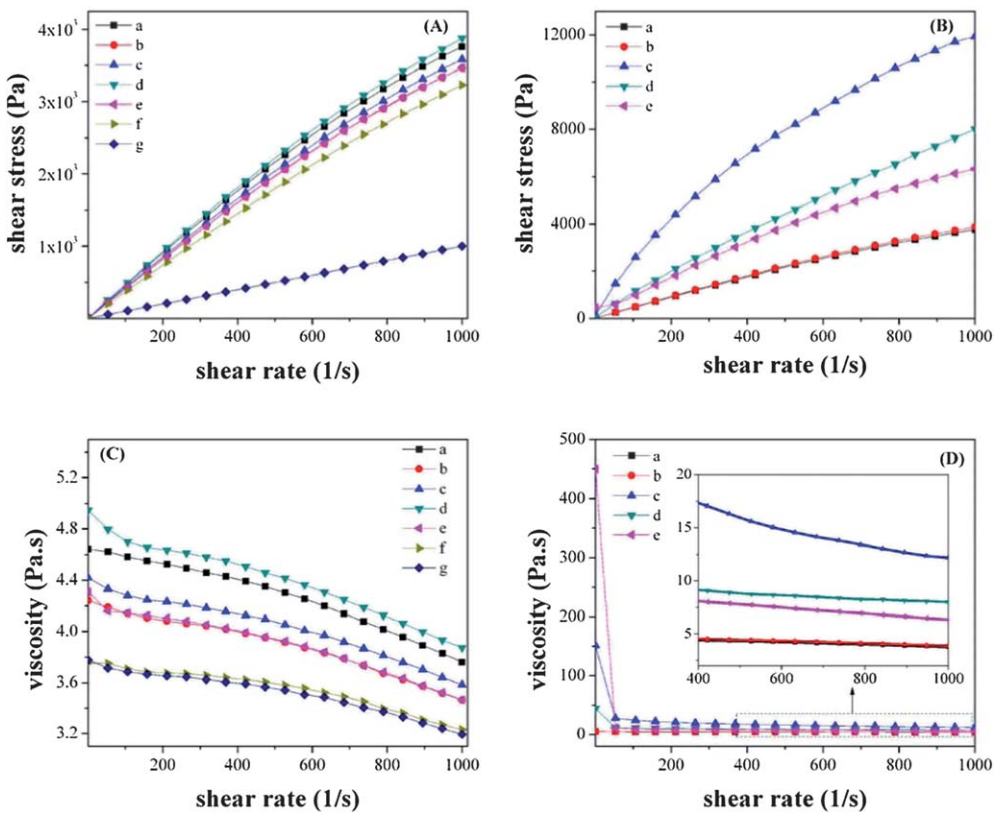

Fig. 1 (A) Shear stress and (C) viscosity *vs.* shear rate of (a) pure epoxy, epoxy nanosuspensions with (b) 1.0 wt% $BaTiO_3$ (500 nm), (c) 5.0 wt% $BaTiO_3$ (500 nm), (d) 10.0 wt% $BaTiO_3$ (500 nm), (e) 1.0 wt% $BaTiO_3$ (100 nm), (f) 5.0 wt% $BaTiO_3$ (100 nm), (g) 10.0 wt% $BaTiO_3$ (100 nm); (B) shear stress and (D) viscosity *vs.* shear rate of (a) pure epoxy, epoxy nanosuspensions with (b) 10.0 wt% $BaTiO_3$ (500 nm), (c) 28.57 wt% $BaTiO_3$ (500 nm)–PANI (contains 10 wt% $BaTiO_3$ and 18.57 wt% PANI), (d) 15.38 wt% $BaTiO_3$ (500 nm)–PANI (contains 5.38 wt% $BaTiO_3$ and 10 wt% PANI) and (e) 10.0 wt% PANI.

Table 1 Flow behavior indices of the liquid epoxy resin and its nanosuspensions with $BaTiO_3$ NPs and $BaTiO_3$–PANI NPs

	Pure epoxy	Nanosuspension with 10 wt% $BaTiO_3$ (500 nm)	Nanosuspension with 28.57 wt% $BaTiO_3$ (500 nm)–PANI (contains 10 wt% $BaTiO_3$ and 18.57 wt% PANI)	Nanosuspension with 15.38 wt% $BaTiO_3$ (500 nm)–PANI (contains 5.38 wt% $BaTiO_3$ and 10 wt% PANI)	Nanosuspension with 10 wt% PANI
n	0.9708	0.9726	0.7493	0.8701	0.8693

viscosity in the limit of zero shear rate,[48] and d is the rate index. It is shown that for both pure epoxy resin ($d = 0.04426$) and the nanosuspension with 10.0 wt% $BaTiO_3$ NPs (500 nm) ($d = 0.07803$), the value of d is almost equal to zero, and a zero d indicates Newtonian behavior.[49] As d equals zero, the viscosity no longer depends on the shear rate, the viscosity remains constant and should be equal to zero shear viscosity with increasing the shear rate. In addition, the value of $1/C$ is considered as the critical shear rate (the shear rate for breaking the structural linkages) and can be applied for evaluating the onset shear rate of shear thinning.[50] The small C values of the Newtonian pure epoxy resin ($C = 0.007454$ s) and the epoxy resin nanosuspension with 10.0 wt% $BaTiO_3$ NPs (500 nm) ($C = 0.05335$ s) indicate that the "shear-thinning" process (due to the sample splashing under high rotating speed of cone) can only be observed in very high shear rate range (134.16 s^{-1}). However, for the pseudoplastic epoxy resin nanosuspensions with 10 wt% PANI ($C = 18.82$ s), 15.38 wt% $BaTiO_3$ (500 nm)–PANI (contains 5.38 wt% $BaTiO_3$ and 10 wt% PANI) ($C = 23.93$ s) and 28.57 wt% $BaTiO_3$ (500 nm)–PANI (contains 10 wt% $BaTiO_3$ and 18.57 wt% PANI) ($C = 33.82$ s), the values of C are much higher and increase with increasing the PANI loading. The larger the C value, the lower the shear rate for the shear thinning process to begin, and the reduced viscosity is beneficial for industrial manufacturing.

Moreover, it is shown in Table 2 that both zero shear viscosity and infinite shear viscosity are also dominated by the loading of $BaTiO_3$ (500 nm)–PANI, and in fact the PANI coating layer. Comparing the zero shear viscosity and infinite shear viscosity of the nanosuspensions with 15.38 wt% $BaTiO_3$ (500 nm)–PANI (contains 5.38 wt% $BaTiO_3$ and 10 wt% PANI) and 10 wt% PANI, the values of both viscosities are almost the same and the largest value of the shear viscosity is observed in the nanosuspension with the highest loading of PANI (28.57 wt% $BaTiO_3$–PANI (contains 10 wt% $BaTiO_3$ and 18.57 wt% PANI)) ($\eta_0 = 935.9$ Pa s, $\eta_\infty = 12.63$ Pa s). All the results of the rheology tests in the steady state indicate that the introduction of a PANI layer on the $BaTiO_3$ nanoparticle surface makes the epoxy resin behavior tend to change from that of a Newtonian fluid to a pseudoplastic fluid, and the extent of pseudoplastic behavior depends on the PANI layer on the $BaTiO_3$ NPs.

The rheological behavior of the nanosuspensions was also studied by the oscillation test. Fig. 2(A) shows the storage modulus (G') and loss modulus (G'') of the epoxy resin nanosuspensions with $BaTiO_3$ and $BaTiO_3$–PANI NPs. Compared with the other three samples containing PANI coating, no crossing point of G' and G'' (with G'' always larger than G' in the whole test range) can be observed in the epoxy nanosuspension with 10.0 wt% $BaTiO_3$, Fig. 2(A)-(a). However, for the epoxy resin nanosuspensions with 10.0 wt% PANI, Fig. 2(A)-(d), 15.38 wt% $BaTiO_3$–PANI (contains 5.38 wt% $BaTiO_3$ and 10.0 wt% PANI) Fig. 2(A)-(c) and 28.57 wt% $BaTiO_3$–PANI (contains 10.0 wt% $BaTiO_3$ and 18.57 wt% PANI) Fig. 2(A)-(b), the crossing points of G' and G'' can be observed at angle frequency (ω) values around 2.3, 1.2 and 50 rad s^{-1}, respectively, and G' is even higher than G'' in the low frequency range. The crossing point of the G' and G'' curves is considered as a criterion to identify the transition from elastic solid behavior to viscous liquid behavior.[44] For the epoxy resin nanosuspensions with bare $BaTiO_3$ NPs without any chemical bonding between the nanofillers and the epoxy resin monomers, the nanosuspensions only show viscous liquid behavior without forming a network and cannot change from viscous liquid to elastic solid with increasing the frequency, which indicates a typical Newtonian fluid with an observed phase angle (δ) (the phase angle between G'' and G') of 90°,[51] Fig. 2(B). However for the nanosuspensions with PANI coating on the $BaTiO_3$ nanoparticle surface, they behave more like an elastic solid rather than a viscous liquid, δ decreases with increasing the loading of $BaTiO_3$ (500 nm)–PANI NPs (as the aforementioned PANI layer on the surface of $BaTiO_3$ NPs), Fig. 2(B). Thus, the PANI coating on the $BaTiO_3$

Table 2 Parameters in the Carreau model for the epoxy resin nanosuspensions with $BaTiO_3$ NPs and polyaniline-coated $BaTiO_3$ NPs

	η_0 (Pa s)	η_∞ (Pa s)	C (s)	d
Pure epoxy	4.638	0.2536	0.007454	0.04426
Epoxy resin nanosuspension with 10.0 wt% $BaTiO_3$ (500 nm)	4.947	3.092	0.05335	0.07803
Epoxy resin nanosuspension with 28.57 wt% $BaTiO_3$–PANI (contains 10 wt% $BaTiO_3$ and 18.57 wt% PANI)	935.9	12.63	33.82	0.5393
Epoxy resin nanosuspension with 15.38 wt% $BaTiO_3$–PANI (contains 5.38 wt% $BaTiO_3$ and 10 wt% PANI)	232.3	8.167	23.93	0.5729
Epoxy resin nanosuspension with 10.0 wt% PANI	238.8	8.001	18.82	1.243

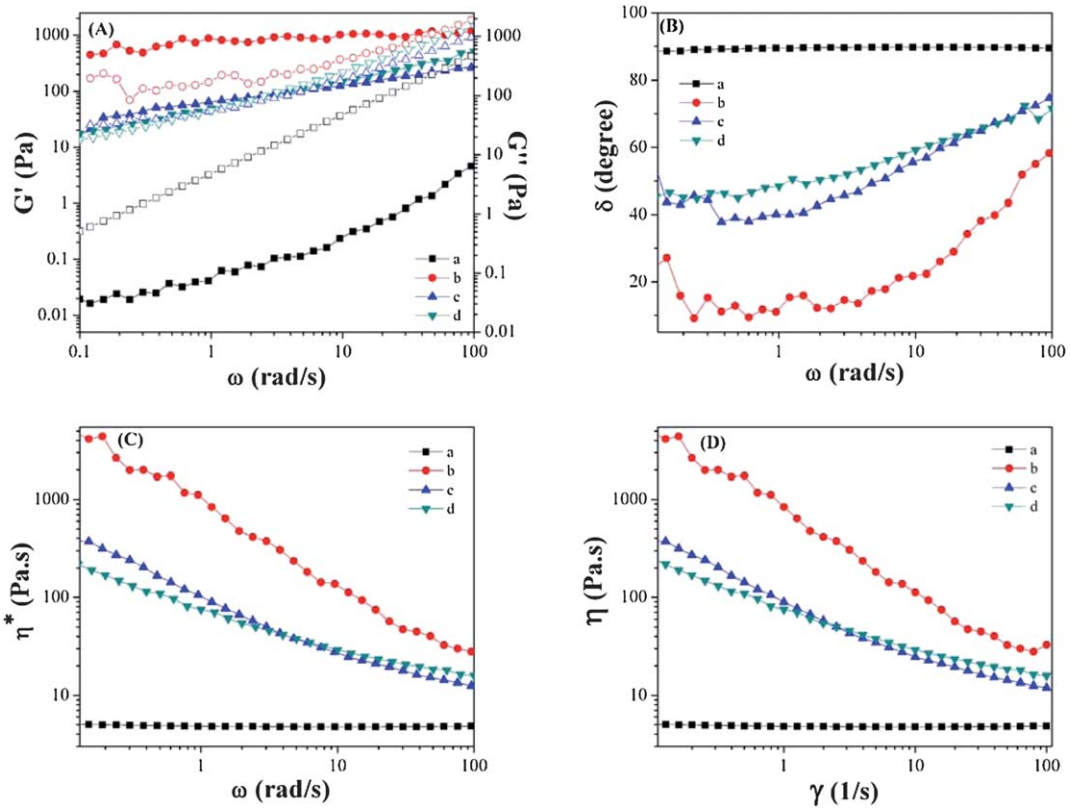

Fig. 2 (A) G' and G'' (solid and open symbols represent G' and G'', respectively), (B) δ, (C) complex viscosity (η^*) *vs.* ω, and (D) viscosity *vs.* shear rate of the epoxy resin nanosuspensions with (a) 10.0 wt% $BaTiO_3$ (500 nm), (b) 28.57 wt% $BaTiO_3$–PANI (contains 10 wt% $BaTiO_3$ and 18.57 wt% PANI), (c) 15.38 wt% $BaTiO_3$–PANI (contains 5.38 wt% $BaTiO_3$ and 10 wt% PANI) and (d) 10.0 wt% PANI.

nanoparticle surface is helpful for the network formation of the epoxy resin.

The complex viscosity ($\eta^* = \eta' - i\eta''$, where $\eta' = G'/\omega$ and $\eta'' = G''/\omega$)[52] of the epoxy resin nanosuspensions was also studied. For the epoxy resin nanosuspension with 10.0 wt% $BaTiO_3$ NPs, the η^* is constant in the whole frequency range, Fig. 2(C). However, for the epoxy resin nanosuspensions with 10.0 wt% PANI, 15.38 wt% $BaTiO_3$–PANI (contains 5.38 wt% $BaTiO_3$ and 10.0 wt% PANI) and 28.57 wt% $BaTiO_3$–PANI (contains 10.0 wt% $BaTiO_3$ and 18.57 wt% PANI), the η^* decreases with increasing frequency, Fig. 2(C). The complex viscosity ($\eta^*(\omega)$) can be transformed to a steady-state viscosity ($\eta(\gamma)$, viscosity obtained from a ramp-strain experiment[53]) and correlated to the shear rate by using the Cox–Merz rule, eqn (3):[54]

$$\eta(\gamma) = \left|\eta^*(\omega)\right|_{\omega=\gamma} = \sqrt{\left[(G'/\omega)^2 + (G''/\omega)^2\right]_{\omega=\gamma}} \quad (3)$$

where G' and G'' are the storage and loss moduli, ω is the angular frequency, and γ is the shear rate.

When $\omega = \gamma$, the value of η^* is equal to that of steady-state viscosity. From Fig. 2(D), the zero shear viscosity (limiting viscosity at zero shear rate,[47] $\eta_0 = \lim_{\gamma \to 0} \eta$) of the epoxy resin nanosuspensions with PANI coating on the $BaTiO_3$ nanoparticle surface is observed to be higher than that of the epoxy resin nanosuspension with 10.0 wt% $BaTiO_3$ NPs and is consistent with the calculations from the Carreau model correlating the viscosity to the shear rate. All the viscosity studies indicate that the PANI coating on the $BaTiO_3$ nanoparticle surface can promote the epoxy resin network formation, which is caused by the reaction between the amine groups in PANI on the $BaTiO_3$ nanoparticle surface and the epoxy resin.[45]

3.2 Thermogravimetric analysis

Fig. 3(A) shows the TGA curves of the cured pure epoxy, as-received $BaTiO_3$ NPs and the PNCs with different sized $BaTiO_3$ NPs in nitrogen. For all the PNCs, there is only one sharp weight loss stage caused by the breaking down of the polymer chains. From the onset decomposition temperature summarized in Table 3, the decomposition temperature firstly decreases with increasing the $BaTiO_3$ (500 nm) nanoparticle loading (1.0 and 5.0 wt%); when the loading of $BaTiO_3$ NPs (500 nm) is further increased (8.0 and 10.0 wt%), the decomposition temperature becomes increased but still lower than that of the cured pure epoxy resin (375.28 °C). For the PNCs with different sized $BaTiO_3$ NPs, the decomposition temperature is almost the same, thus the particle size has no significant influence on the thermal stability of the PNCs. Compared with the cured pure epoxy, the introduction of NPs decreases the curing extent of the epoxy resin[55] and thus the network structure of PNCs was not well formed and would be easily broken down with increasing temperature, which causes a decreased decomposition temperature.[56] For the PNCs with

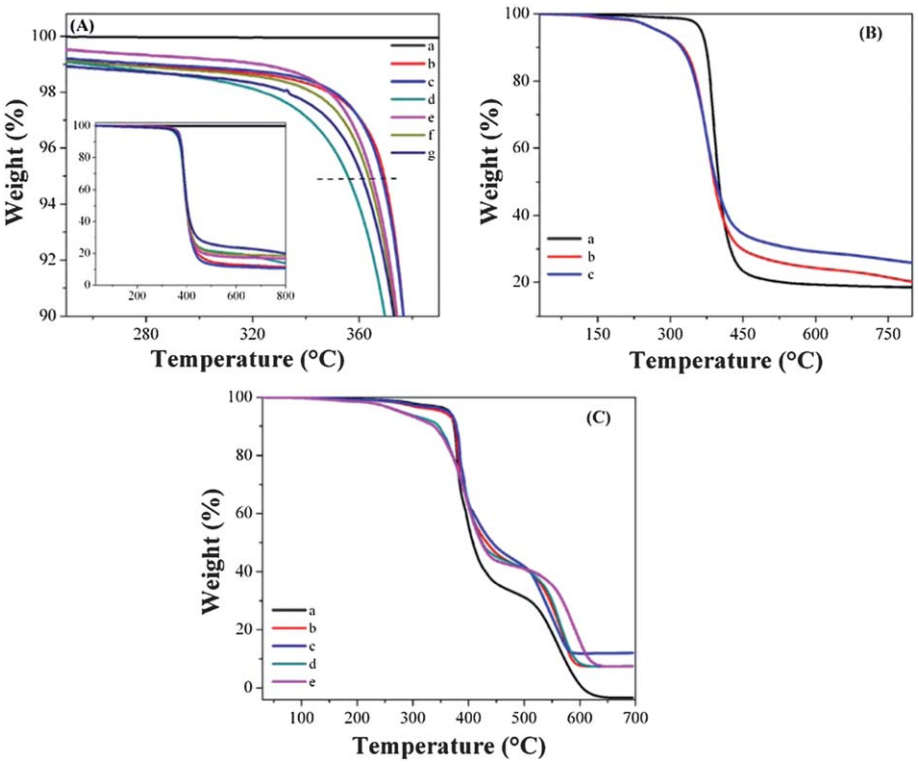

Fig. 3 (A) TGA curves of (a) pure $BaTiO_3$ NPs, (b) cured pure epoxy and the PNCs with (c) 1.0 wt% $BaTiO_3$ (500 nm), (d) 5.0 wt% $BaTiO_3$ (500 nm), (e) 8.0 wt% $BaTiO_3$ (500 nm), (f) 10.0 wt% $BaTiO_3$ (500 nm) and (g) 10.0 wt% $BaTiO_3$ (100 nm) in nitrogen; (B) TGA curves of the PNCs with (a) 10.0 wt% $BaTiO_3$ (500 nm), (b) 28.57 wt% $BaTiO_3$–PANI (contains 10 wt% $BaTiO_3$ and 18.57 wt% PANI) and (c) 15.38 wt% $BaTiO_3$–PANI (contains 5.38 wt% $BaTiO_3$ and 10 wt% PANI) in nitrogen; (C) TGA curves of (a) cured pure epoxy and the PNCs with (b) 10.0 wt% $BaTiO_3$ (500 nm), (c) 10.0 wt% $BaTiO_3$ (100 nm), (d) 28.57 wt% $BaTiO_3$–PANI (contains 10 wt% $BaTiO_3$ and 18.57 wt% PANI) and (e) 15.38 wt% $BaTiO_3$–PANI (contains 5.38 wt% $BaTiO_3$ and 10 wt% PANI) in air.

the $BaTiO_3$–PANI NPs (Fig. 3(B)), a reduced onset decomposition temperature is observed resulting from the lower onset decomposition temperature of pure PANI, which is due to the release of moisture and organic solvent residue entangled in the PANI polymer chains.[2] However, when the test was run in air, Fig. 3(C), two weight loss stages were observed. The first degradation stage in air is almost the same as that in the nitrogen case, which is associated with the breaking of the crosslinked network in epoxy. However, the second stage stems from the structure conversion or oxidation of the aromatic rings in epoxy,[57] and all the PNCs show a higher onset decomposition temperature than the cured pure epoxy in this stage, Table 4. The mechanisms of the enhanced thermal stability are associated with the protection effect of the $BaTiO_3$ NPs and the restricted decomposition function of the $BaTiO_3$–PANI NPs. For the PNCs with $BaTiO_3$ NPs, the NPs can act as a shield and separate the polymer chains from heat.[1] On the other hand, for the PNCs with the $BaTiO_3$–PANI NPs, the increased onset decomposition temperature is attributed to the covalent bonds formed between the amine groups in PANI and the epoxy resin,[52] which can postpone the breakdown of the aromatic rings.[58] The enhanced thermal stability can also be observed in the flammability analysis, Fig. 4.

Table 3 Onset decomposition temperature, weight loss at 800 °C under nitrogen and glass transition temperature of the cured pure epoxy and its cured nanocomposites

Sample name	Onset temperature (°C)	Weight loss (%)	T_g (°C)
Pure epoxy	375.28	88.02	108.31
PNC with 1.0 wt% $BaTiO_3$ (500 nm)	374.35	89.06	54.10
PNC with 5.0 wt% $BaTiO_3$ (500 nm)	370.48	86.12	78.34
PNC with 8.0 wt% $BaTiO_3$ (500 nm)	372.58	82.97	82.47
PNC with 10.0 wt% $BaTiO_3$ (500 nm)	373.00	81.51	82.77
PNC with 10.0 wt% $BaTiO_3$ (100 nm)	373.39	90.89	79.78
PNC with 15.38 wt% $BaTiO_3$–PANI (contains 5.38 wt% $BaTiO_3$ and 10 wt% PANI)	239.92	79.40	89.62
PNC with 28.57 wt% $BaTiO_3$–PANI (contains 10 wt% $BaTiO_3$ and 18.57 wt% PANI)	233.77	73.88	95.98

Table 4 First onset temperature in the temperature range between 200 and 400 °C and the second onset temperature in the temperature range between 450 and 600 °C in air for the cured pure epoxy and its nanocomposites

Sample name	First onset temperature (°C)	Second onset temperature (°C)	Weight loss (%)
Cured pure epoxy	243.22	524.42	103.2
PNC with 10.0 wt% $BaTiO_3$ (500 nm)	266.51	525.71	92.50
PNC with 10.0 wt% $BaTiO_3$ (100 nm)	264.73	524.96	87.79
PNC with 15.38 wt% $BaTiO_3$–PANI (contains 5.38 wt% $BaTiO_3$ and 10 wt% PANI)	228.31	530.39	92.19
PNC with 28.57 wt% $BaTiO_3$–PANI (contains 10 wt% $BaTiO_3$ and 18.57 wt% PANI)	224.59	550.07	92.35

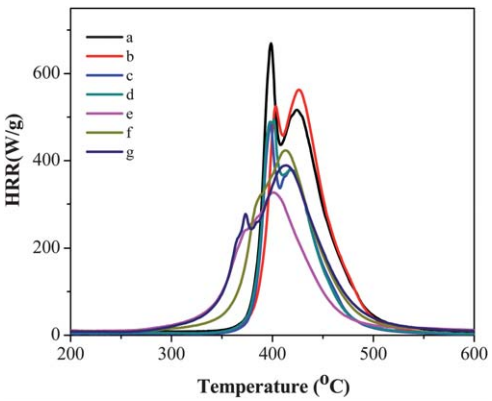

Fig. 4 The HRR *vs.* temperature curves of (a) the cured pure epoxy and its PNCs with (b) 1.0 wt% $BaTiO_3$ (500 nm), (c) 10.0 wt% $BaTiO_3$ (500 nm), (d) 10.0 wt% $BaTiO_3$ (100 nm), (e) 28.57 wt% $BaTiO_3$–PANI (contains 10 wt% $BaTiO_3$ and 18.57 wt% PANI) and (f) 15.38 wt% $BaTiO_3$–PANI (contains 5.38 wt% $BaTiO_3$ and 10 wt% PANI), (g) 10.0 wt% PANI.

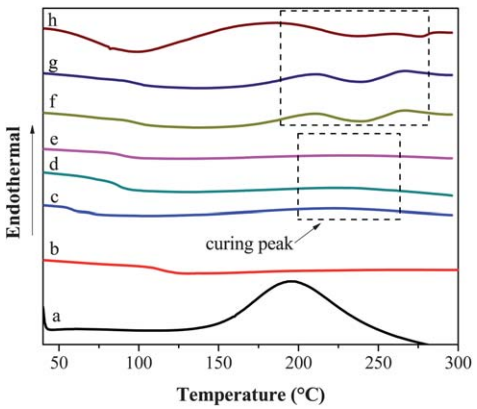

Fig. 5 DSC curves of (a) the mixture of pure epoxy resin and curing agent, (b) cured pure epoxy and cured PNCs with (c) 1.0 wt% $BaTiO_3$ (500 nm), (d) 5.0 wt% $BaTiO_3$ (500 nm), (e) 10.0 wt% $BaTiO_3$ (500 nm), (f) 28.57 wt% $BaTiO_3$–PANI (contains 10 wt% $BaTiO_3$ and 18.57 wt% PANI) and (g) 15.38 wt% $BaTiO_3$–PANI (contains 5.38 wt% $BaTiO_3$ and 10 wt% PANI); (h) pure $BaTiO_3$–PANI NPs.

3.3 Flammability analysis

The flammability behaviors of the cured PNCs filled with $BaTiO_3$ and $BaTiO_3$–PANI NPs were evaluated by studying the heat release capacity (HR capacity), peak heat release rate (pHRR), total heat release and char residue, which are summarized in Table 5. From the curve of heat release rate (HRR) as a function of temperature, Fig. 4, the pHRR, HR capacity and total HR of the PNCs decrease with increasing the $BaTiO_3$ nanoparticle loading, indicating that the existence of the $BaTiO_3$ NPs reduced the heat release from the cured epoxy resin. The inorganic NPs are well used as flame retardant additives to enhance the thermal stability of the polymer matrix by forming a continuous network structure, which can serve as a protecting layer to prevent the heat transfer to the inner part.[1] At the same loading level of the $BaTiO_3$ NPs, the PNCs with small $BaTiO_3$ NPs exhibit almost the same pHRR value as that of the

Table 5 Heat release capacity (HR capacity), peak heat release rate (pHRR), total heat release and char residue for cured pure epoxy and its PNCs

	HR capacity ($J\ g^{-1}\ K^{-1}$)	pHRR ($W\ g^{-1}$)	Total HR ($kJ\ g^{-1}$)	Char residue (%)
Pure epoxy	491	664.3	28	12
Pure PANI	73	77.69	11.9	51
PNCs with 1.0 wt% $BaTiO_3$ (500 nm)	417	560.2	26.4	12
PNCs with 10.0 wt% $BaTiO_3$ (500 nm)	454	483.2	23.8	15
PNCs with 10.0 wt% $BaTiO_3$ (100 nm)	459	484.9	24.5	16
PNCs with 28.57 wt% $BaTiO_3$/PANI (contains 10 wt% $BaTiO_3$ and 18.57 wt% PANI)	239	317.2	19.4	25
PNCs with 15.38 wt% $BaTiO_3$/PANI (contains 5.38 wt% $BaTiO_3$ and 10 wt% PANI)	311	414.7	22.8	20
PNCs with 10.0 wt% PANI	285	381	24.9	18

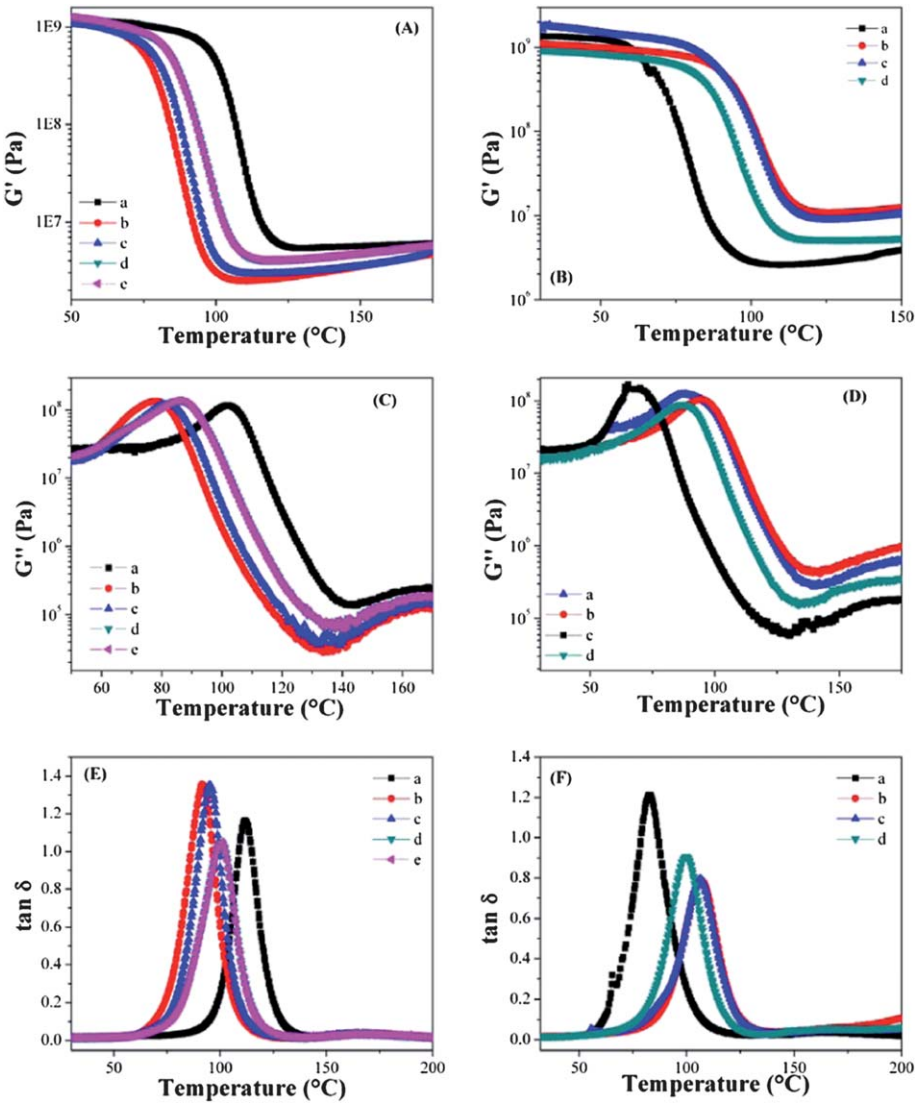

Fig. 6 (A) Storage modulus (*G′*), (C) loss modulus (*G″*) and (E) tan *δ vs.* temperature of (a) cured pure epoxy, and PNCs with (b) 1.0 wt% $BaTiO_3$ (500 nm), (c) 5.0 wt% $BaTiO_3$ (500 nm), (d) 8.0 wt% $BaTiO_3$ (500 nm) and (e) 8.0 wt% $BaTiO_3$ (100 nm), curves (d) and (e) are overlapped; (B) storage modulus (*G′*), (D) loss modulus (*G″*) and (F) tan *δ vs.* temperature of PNCs with (a) 10.0 wt% $BaTiO_3$ (500 nm), (b) 28.57 wt% $BaTiO_3$–PANI (contains 10 wt% $BaTiO_3$ and 18.57 wt% PANI), (c) 15.38 wt% $BaTiO_3$–PANI (contains 5.38 wt% $BaTiO_3$ and 10.0 wt% PANI) and (d) 10.0 wt% PANI NPs.

PNCs with big $BaTiO_3$ NPs, indicating that the size of $BaTiO_3$ NPs has no effect on the heat release of the PNCs.

The PNCs with 28.57 wt% $BaTiO_3$–PANI (contains 10.0 wt% $BaTiO_3$ and 18.57 wt% PANI) NPs have much lower HRR than those with 10.0 wt% $BaTiO_3$ NPs, indicating that the HRR value mainly depends on the PANI coating. As mentioned in the TGA part, the amine groups in PANI can form covalent bonds with the epoxy matrix, which can postpone the breakdown of the aromatic rings,[58] thus the decreased HRR should be associated with the interfacial reaction between PANI and epoxy resin.[6] The observed reduced HRR in the PNCs with 28.57 wt% $BaTiO_3$–PANI (contains 10.0 wt% $BaTiO_3$ and 18.57 wt% PANI) indicates that the PANI layer on the surface of $BaTiO_3$ NPs in the PNCs inhibited the matrix from pyrolysis. It is known that the existence of PANI can help to form carbonaceous components,[59] and the enhanced char residue indicates that the addition of PANI on the $BaTiO_3$ nanoparticle surface favors the char formation of epoxy matrix. The char yield is considered as a denotation of flame retardancy, the formation of char on the surface of materials can prevent the heat being transferred from the heat source to the inner material[21] and also obstruct the distribution of combustible gases produced during the burning process.[60]

3.4 Differential scanning calorimetry

For the thermosetting systems, gelation, curing, vitrification and devitrification events can be studied with the DSC tests.[61] In general, the former two processes can be observed in the uncured samples, however, if the material is not fully cured, an exothermal peak, which represents the curing process, will be observed for the cured samples. Compared with the cured

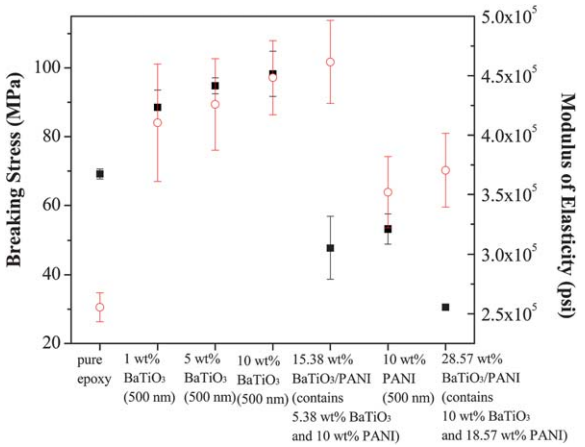

Fig. 7 Breaking tensile stress (solid symbols) and modulus (open symbols) of elasticity of the cured pure epoxy and its PNCs.

pure epoxy, which is observed to be well cured without any exothermal peak, the broad exothermal peaks can be found in the PNC samples with low $BaTiO_3$ nanoparticle loadings (1.0 and 5.0 wt%), however, the peak area becomes smaller in the PNCs with higher loading (10.0 wt%), Fig. 5. Based on the discussion in the TGA part, the existence of the $BaTiO_3$ NPs would limit the curing extent of the epoxy resin, thus in the PNCs, some polymer networks are not completely formed.[56] In the DSC test, with the temperature increasing higher than T_g (Fig. 5), the polymer segment can move again and accomplish the curing process, and the additional curing process is observed in the DSC curve. The curing extent of the PNCs is calculated based on the value of residual heat of curing, eqn (4):[62]

$$\alpha = 1 - \frac{\Delta H}{(1 - w_p)\Delta H_{uc}} \quad (4)$$

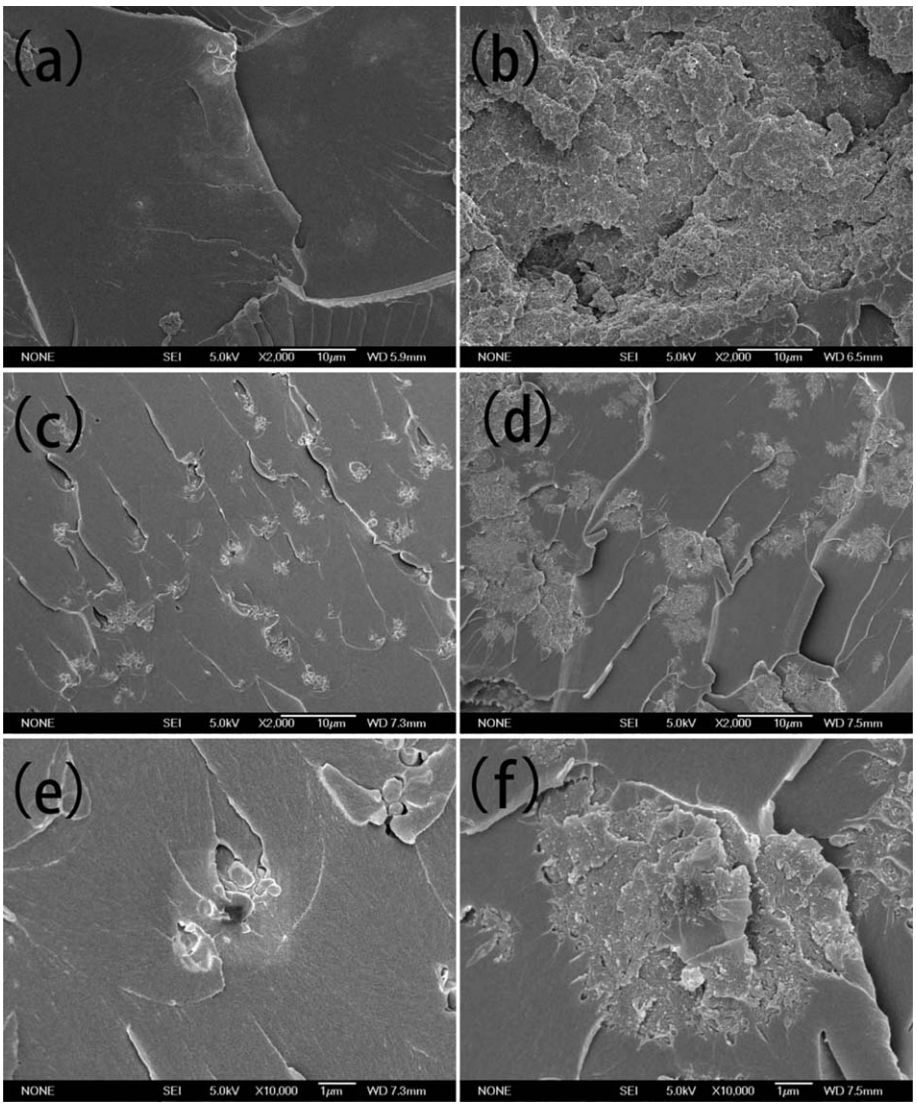

Fig. 8 SEM images of the fracture surface of (a) the cured pure epoxy, and the PNCs with (b) 10.0 wt% PANI NPs, (c and e) 10.0 wt% $BaTiO_3$ NPs (500 run), and (d and f) 28.57 wt% $BaTiO_3$–PANI (contains 10 wt% $BaTiO_3$ and 18.57 wt% PANI).

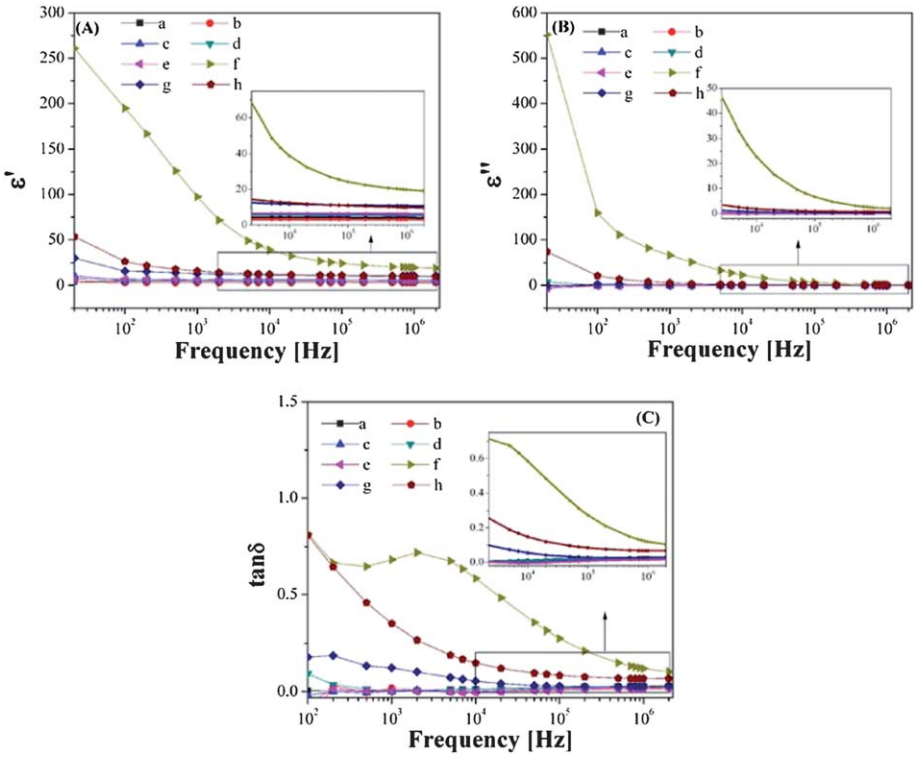

Fig. 9 (A) Real permittivity (ε'), (B) imaginary permittivity (ε''), and (C) dielectric loss (tan δ) of (a) the cured pure epoxy and its PNCs with (b) 1.0 wt% $BaTiO_3$ (500 nm), (c) 5.0 wt% $BaTiO_3$ (500 nm), (d) 5.0 wt% $BaTiO_3$ (100 nm), (e) 10.0 wt% $BaTiO_3$ (500 nm), (f) 28.57 wt% $BaTiO_3$–PANI (contains 10 wt% $BaTiO_3$ and 18.57 wt% PANI), (g) 15.38 wt% $BaTiO_3$–PANI (contains 5.38 wt% $BaTiO_3$ and 10 wt% PANI) and (h) 10.0 wt% PANI NPs.

where ΔH is the residual heat of the reaction in PNCs (J g^{-1}), w_p is the particle weight percentage in the composites and ΔH_{uc} is the residual heat of the uncured pure resin (J g^{-1}). With increasing the $BaTiO_3$ nanoparticle loading, both the value of curing extent (0.83, 0.85 and 0.92 for PNCs with 1.0, 5.0 and 10.0 wt% $BaTiO_3$ NPs) and the T_g of the cured PNCs increases (Table 3). For the liquid uncured thermosetting polymers, with the curing process proceeding, the mobility of the segments would decrease and the T_g would increase, and when the T_g becomes higher than the curing temperature, the reaction would terminate due to the "frozen polymer chain".[63] For the epoxy resin with $BaTiO_3$ NPs, the NPs obstruct the formation of the highly cross-linked molecular structure of epoxy,[64,65] however, the addition of NPs can enhance the mobility of the segment by increasing the free volume between the NPs and the polymer matrix,[66] which favors the curing process.[67] Generally, compared to the PNCs with lower nanoparticle loading (1.0 and 5.0 wt%), the PNCs with higher loading (10.0 wt%) can improve the curing process by increasing the free volume, however, the curing extent of PNCs is still lower than that of the pure epoxy resin, indicating that the introduction of NPs has a negative effect on the curing process of the epoxy matrix.

In addition, for the PNCs with the $BaTiO_3$–PANI NPs, no exothermal peak can be observed and the endothermic peak in the high temperature range is due to the loss of the doping acid in PANI,[68] which can be also tracked from the curve of pure $BaTiO_3$–PANI NPs, Fig. 5 (refer to ESI† for the enlarged DSC curves for c, d and e). The enhanced curing extent of the PNCs with PANI on the $BaTiO_3$ nanoparticle surface resulted from the formed covalent bonds between the epoxy matrix and the amine groups in PANI.[58] The existence of NPs in the cured epoxy resin is observed to cause a decreased glass transition temperature (T_g) compared with cured pure epoxy. The reduced T_g is related to the enlarged free volume and the decreased curing extent.[69] In cured PNCs, larger free volume would arise from the surface between the fillers and the epoxy resin,[66] which provides more space for the polymer chain segments to move even at a lower temperature. Meanwhile, the T_g would decrease with the reduction of curing extent, thus the addition of NPs in the PNCs would cause a reduced T_g; in addition, due to the increased curing extent, the PNCs with higher loading of $BaTiO_3$ nanoparticle (10.0 wt%) show higher T_g than that of the PNCs with lower loading of $BaTiO_3$ nanoparticles (1.0 and 5.0 wt%).

3.5 Dynamic mechanical properties

Dynamic mechanical analysis (DMA) provides information on the storage modulus (G'), loss modulus (G'') and tan δ in the test temperature range. The storage modulus represents the elastic behavior of the materials and the energy storage during the elastic deformation, while the loss modulus reflects the viscous behavior of the materials and the energy dissipation during the test.[5,70] Fig. 6(A–D) show the storage modulus and loss modulus of the cured pure epoxy resin and its nanocomposites. For samples of the cured epoxy nanocomposites

with $BaTiO_3$ NPs (Fig. 6(A and C)), in the glassy plateau, the polymer chains and segments are "frozen" and cannot make any movement, the values of the storage modulus are larger than those of the loss modulus, and no obvious difference can be observed among all the samples; however, with the temperature increases, the onset temperatures for the PNCs to enter the glass transition phase (at which temperature the values of both G' and G'' rapidly changed) are lower than that of the cured pure epoxy. Based on the discussion in the DSC part, the curing process is limited by the NPs that cause the network to form not as well as that in the cured pure epoxy, the glass transition of the PNCs will take place in a lower temperature range than that in the cured pure epoxy. The tan δ value is the ratio of the loss modulus to the storage modulus, and the peak of tan δ is often used to determine the T_g. As shown in Fig. 6(E), for the PNCs with the as-received $BaTiO_3$ NPs, the T_g is decreased compared with that of the cured pure epoxy resin and the T_g is almost the same in the PNCs with different sized $BaTiO_3$ NPs. The reduced T_g, which is consistent with the result in the DSC test, is owing to the reduced curing extent and the enlarged free volume induced by the nanofillers.[66] However, with further temperature increases, the materials enter the rubber plateau, and the loss moduli of all the PNCs are lower than that of the cured pure epoxy, indicating that the addition of the NPs can reduce the friction of polymer chains in the rubber state.[71]

However, for the PNCs with the PANI coating on the $BaTiO_3$ NPs (Fig. 6(B, D and F)), the PANI coating on the $BaTiO_3$ nanoparticle surface can improve the dynamic mechanical properties of the PNCs, compared with the PNCs with 10.0 wt% as-received $BaTiO_3$ NPs, both storage and loss moduli of the PNCs with 28.57 wt% $BaTiO_3$–PANI (contains 10.0 wt% $BaTiO_3$ and 18.57 wt% PANI) would sharply increase at a higher temperature and the enhanced thermal stability is due to the formed covalent bonds between the epoxy matrix and the amine groups in PANI, which can restrain the movement of epoxy chains.[58] In addition, in the rubber state, the PNCs with 28.57 wt% $BaTiO_3$–PANI (contains 10.0 wt% $BaTiO_3$ and 18.57 wt% PANI) have the highest storage and loss moduli, and the enhanced values of both moduli result from the network formed in the PNCs. Due to the restrained movement of the epoxy chains in the PNCs, the friction between polymer chains is increased and causes the enlarged loss modulus, Fig. 6(D). At the same time, the network formed in the PNCs can increase the elastic properties of the PNCs and yield an improved storage modulus, Fig. 6(B).

3.6 Tensile properties and fracture surface of the PNCs

The breaking tensile stress and the modulus of elasticity as a function of $BaTiO_3$ NPs and $BaTiO_3$–PANI NPs are shown in Fig. 7. When the loading of $BaTiO_3$ nanoparticles increases, the stress increases. The fracture surface is very smooth for the cured pure epoxy samples, Fig. 8, and can be considered as a typical brittle fracture with a fracture surface that is smooth and mirror-like.[72] However, for the PNCs with the as-received $BaTiO_3$ NPs, Fig. 8(b), the fracture surface is much rougher than that of the cured pure epoxy, the laminated cracks can be observed on the fracture surface. When the crack extended from one layer to another, energy would be absorbed[73] and cause the increase in the strength and modulus. However, for the PNCs with $BaTiO_3$–PANI NPs, the stress value is much lower than that of the cured pure epoxy, Fig. 7. For the PNCs with the PANI coated $BaTiO_3$ NPs, although the chemical bonds can form between PANI and epoxy resin, the SEM image (Fig. 8(d)) shows that the $BaTiO_3$–PANI NPs are not uniformly dispersed in the epoxy matrix; a similar phenomenon can also be observed in the epoxy resin nanopolymers filled with pure PANI NPs. Due to the polarity difference, PANI (highly polar) tends to agglomerate in the non-polar matrix,[74] and thus the PANI coating layer on the surface of $BaTiO_3$ NPs would cause some extent of agglomeration in the epoxy resin, which is also shown in the SEM image. Compared with the as-received $BaTiO_3$ NPs (Fig. 8(c and e)), the $BaTiO_3$–PANI NPs (Fig. 8(d and f)) have poor dispersion in the matrix, and the particle-rich regions can cause defects and initiate the failure in epoxy resin.[52] Thus the PANI layer of $BaTiO_3$–PANI NPs would decrease the tensile strength of the PNCs.[52,74]

3.7 Dielectric permittivity

For the dielectric behavior study, the real permittivity, imaginary permittivity and dielectric loss are shown in Fig. 9. For all the samples, both real permittivity and imaginary permittivity decrease with increasing frequency due to the dipolar groups, which cannot follow the speed of the alternating electric field.[75] At lower frequency, the dipolar functional groups can orient themselves and thus a high permittivity value is observed,[75] however, the dipolar groups cannot orient at the same rate as the alternating electric field at higher frequency and thus cause a reduced permittivity.[75] For the PNCs with the $BaTiO_3$ NPs, with increasing the nanoparticle loading, the values of both real and imaginary permittivity increase, and for the PNCs with different sizes of $BaTiO_3$ NPs, the permittivity values are almost the same. The enhanced dielectric behavior is due to the ferroelectric nature (materials exhibit a spontaneous electric polarization that can be reversed by an external field[76]) of $BaTiO_3$, indicating that the $BaTiO_3$ NPs can store charge and hence cause an increased permittivity.[2] However, the highest permittivity value is observed in the PNCs with the 28.57 wt% $BaTiO_3$–PANI (contains 10.0 wt% $BaTiO_3$ and 18.57 wt% PANI) NPs. The high positive permittivity in the PNCs is due to the interfacial polarization,[77] which arises from the charge carriers blocked at the internal surface or interfaces between matrix and fillers.[78] In the PANI coating layer on the $BaTiO_3$ nanoparticle surface, the protons (hydrogen ions) provided by the doping acid can move along the PANI chains, however, these charge movements will be hindered by the $BaTiO_3$ NPs and epoxy resin, resulting in large space charges accumulated in the interface of PANI and $BaTiO_3$ NPs (or epoxy) to give a large interfacial polarization.[79,80] The observed much higher tan δ of the PNCs than that of the cured pure epoxy, Fig. 9(C), is associated with the free charge motion difference,[80] indicating an interfacial polarization formed in the PNCs.

4 Conclusions

The epoxy polymer nanocomposites with both the as-received $BaTiO_3$ (500 and 100 nm) and the PANI coated $BaTiO_3$ NPs at different loading levels have been prepared and systematically studied. Both viscosity and complex viscosity are studied in the rheology test and the results indicate that the amine groups in the PANI layer of $BaTiO_3$–PANI NPs can react with the epoxy resin, and promote the network formation of epoxy resin. Although the nanofillers caused the onset decomposition temperature decrease in nitrogen, it postponed the breakdown of the aromatic rings in air. The flammability studies have successfully demonstrated that the introduction of the nanofillers can decrease the heat release rate of epoxy resin and increase the char residue. The dynamic storage and loss moduli were studied together with the glass transition temperature (T_g) obtained from the peak of tan δ. Compared to pure epoxy resin, the reduced T_g in the PNCs is associated with the reduced curing extent and the enlarged free volume. The enhanced storage modulus in the PNCs with $BaTiO_3$–PANI is associated with the formed covalent bonds between epoxy matrix and the amine groups in PANI, which can restrain the movements of the epoxy chains. More laminated cracks are observed on the fracture surface of the PNCs. The crack extension from one layer to the other causing the energy adsorption contributed to the enhanced modulus of elasticity. Compared with the cured pure epoxy, the improved dielectric behavior of the PNCs is attributed to the ferroelectric nature of $BaTiO_3$ and the large interfacial polarization.

Acknowledgements

This project is supported by the National Science Foundation-Nanoscale Interdisciplinary Research Team and Materials Processing and Manufacturing (CMMI 10-30755) managed by Dr Mary Toney. S. Wei acknowledges the Welch foundation (V-0004).

References

1 T. Kashiwagi, F. Du, J. F. Douglas, K. I. Winey, R. H. Harris and J. R. Shields, *Nat. Mater.*, 2005, **4**, 928.
2 X. Zhang, S. Wei, N. Haldolaarachchige, H. A. Colorado, Z. Luo, D. P. Young and Z. Guo, *J. Phys. Chem. C*, 2012, **116**, 5731.
3 J. Deng, X. Ding, W. Zhang, Y. Peng, J. Wang, X. Long, P. Li and A. S. C. Chan, *Polymer*, 2002, **43**, 2179.
4 J. Zhu, S. Wei, L. Zhang, Y. Mao, J. Ryu, A. B. Karki, D. P. Young and Z. Guo, *J. Mater. Chem.*, 2011, **21**, 342.
5 J. Zhu, S. Wei, J. Ryu, M. Budhathoki, G. Liang and Z. Guo, *J. Mater. Chem.*, 2010, **20**, 4937.
6 H. Gu, S. Tadakamalla, Y. Huang, H. A. Colorado, Z. Luo, N. Haldolaarachchige, D. P. Young, S. Wei and Z. Guo, *ACS Appl. Mater. Interfaces*, 2012, **4**, 5613.
7 B. Chu, X. Zhou, K. Ren, B. Neese, M. Lin, Q. Wang, F. Bauer and Q. M. Zhang, *Science*, 2006, **313**, 334.
8 H. Fu and L. Bellaiche, *Phys. Rev. Lett.*, 2003, **91**, 257601.
9 S. Roberts, *Phys. Rev. Lett.*, 1947, **71**, 890.
10 H. Windlass, P. M. Raj, D. Balaraman, S. K. Bhattacharya and R. R. Tummala, *IEEE Trans. Electron. Packag. Manuf.*, 2003, **26**, 100.
11 Y. Kobayashi, T. Tanase, T. Tabata, T. Miwa and M. Konno, *J. Eur. Ceram. Soc.*, 2008, **28**, 117.
12 Y. Kobayashi, A. Kosuge and M. Konno, *Appl. Surf. Sci.*, 2008, **255**, 2723.
13 J. Wang, Q. Lin, R. Zhou and B. Xu, *Sens. Actuators, B*, 2002, **81**, 248.
14 H. M. Jung, J.-H. Kang, S. Y. Yang, J. C. Won and Y. S. Kim, *Chem. Mater.*, 2009, **22**, 450.
15 J. A. Mikroyannidis and D. A. Kourtides, *J. Appl. Polym. Sci.*, 1984, **29**, 197.
16 X. Zhang, F. Guo, J. Chen, G. Wang and H. Liu, *Polym. Degrad. Stab.*, 2005, **87**, 411.
17 W. Chen and B. Qu, *Chem. Mater.*, 2003, **15**, 3208.
18 S. Zhang, A. R. Horrocks, R. Hull and B. K. Kandola, *Polym. Degrad. Stab.*, 2006, **91**, 719.
19 Y. Hu, S. Wang, Z. Ling, Y. Zhuang, Z. Chen and W. Fan, *Macromol. Mater. Eng.*, 2003, **288**, 272.
20 M. Zammarano, M. Franceschi, S. v. Bellayer, J. W. Gilman and S. Meriani, *Polymer*, 2005, **46**, 9314.
21 J. W. Gilman, *Appl. Clay Sci.*, 1999, **15**, 31.
22 J. W. Gilman, C. L. Jackson, A. B. Morgan, R. Harris, E. Manias, E. P. Giannelis, M. Wuthenow, D. Hilton and S. H. Phillips, *Chem. Mater.*, 2000, **12**, 1866.
23 Q. Sun, F. J. Schork and Y. Deng, *Compos. Sci. Technol.*, 2007, **67**, 1823.
24 W. Lertwimolnun and B. Vergnes, *Polymer*, 2005, **46**, 3462.
25 S.-Y. Lu and I. Hamerton, *Prog. Polym. Sci.*, 2002, **27**, 1661.
26 P. Kiliaris and C. D. Papaspyrides, *Prog. Polym. Sci.*, 2010, **35**, 902.
27 F. Laoutid, L. Bonnaud, M. Alexandre, J. M. Lopez-Cuesta and P. Dubois, *Mater. Sci. Eng., R*, 2009, **63**, 100.
28 H.-S. Moon and J.-K. Park, *Synth. Met.*, 1998, **92**, 223.
29 J. Tarver, J. E. Yoo, T. J. Dennes, J. Schwartz and Y.-L. Loo, *Chem. Mater.*, 2008, **21**, 280.
30 J. E. Yoo, J. L. Cross, T. L. Bucholz, K. S. Lee, M. P. Espe and Y.-L. Loo, *J. Mater. Chem.*, 2007, **17**, 1268.
31 X. Yang, B. Li, H. Wang and B. Hou, *Prog. Org. Coat.*, 2010, **69**, 267.
32 S. K. Dhawan, D. Kumar, M. K. Ram, S. Chandra and D. C. Trivedi, *Sens. Actuators, B*, 1997, **40**, 99.
33 A. Olad and R. Nabavi, *J. Hazard. Mater.*, 2007, **147**, 845.
34 H. Gu, S. Rapole, J. Sharma, Y. Huang, D. Cao, H. Colorado, Z. Luo, N. Haldolaarachchige, D. P. Young, B. Walters, S. Wei and Z. Guo, *RSC Adv.*, 2012, **2**, 11007.
35 M. Li, Y. Guo, Y. Wei, A. G. MacDiarmid and P. I. Lelkes, *Biomaterials*, 2006, **27**, 2705.
36 H. Wei, X. Yan, S. Wu, Z. Luo, S. Wei and Z. Guo, *J. Phys. Chem. C*, 2012, **116**, 25052.
37 J. Zhu, M. Chen, H. Qu, X. Zhang, H. Wei, Z. Luo, H. A. Colorado, S. Wei and Z. Guo, *Polymer*, 2012, **53**, 5953.
38 H. Wei, J. Zhu, S. Wu, S. Wei and Z. Guo, *Polymer*, 2013, **54**, 1820.

39 H. C. Pant, M. K. Patra, A. Verma, S. R. Vadera and N. Kumar, *Acta Mater.*, 2006, **54**, 3163.
40 J. H. Wei, J. Shi, J. G. Guan and R. Z. Yuan, *J. Mater. Sci.*, 2004, **39**, 3457.
41 J. Zhu, S. Wei, L. Zhang, Y. Mao, J. Ryu, N. Haldolaarachchige, D. P. Young and Z. Guo, *J. Mater. Chem.*, 2011, **21**, 3952.
42 R. M. Manglik and P. Fang, *Int. J. Heat Mass Transfer*, 2002, **45**, 803.
43 A. Tuteja, P. M. Duxbury and M. E. Mackay, *Macromolecules*, 2007, **40**, 9427.
44 J. Zhu, S. Wei, A. Yadav and Z. Guo, *Polymer*, 2010, **51**, 2643.
45 X. Zhang, Q. He, H. Gu, H. A. Colorado, S. Wei and Z. Guo, *ACS Appl. Mater. Interfaces*, 2013, **5**, 898.
46 Y. H. Hyun, S. T. Lim, H. J. Choi and M. S. Jhon, *Macromolecules*, 2001, **34**, 8084.
47 M. M. Cross, *J. Colloid Sci.*, 1965, **20**, 417.
48 K. Khellaf and G. Lauriat, *J. Non-Newtonian Fluid Mech.*, 2000, **89**, 45.
49 S. H. Park, S. T. Lim, T. K. Shin, H. J. Choi and M. S. Jhon, *Polymer*, 2001, **42**, 5737.
50 J. Zhu, S. Wei, J. Ryu, L. Sun, Z. Luo and Z. Guo, *ACS Appl. Mater. Interfaces*, 2010, **2**, 2100.
51 H. B. Dick, F. Krummenauer, A. J. Augustin, T. Pakula and N. Pfeiffer, *J. Cataract Refractive Surg.*, 2001, **27**, 320.
52 H. Gu, S. Tadakamalla, X. Zhang, Y.-D. Huang, Y. Jiang, H. A. Colorado, Z. Luo, S. Wei and Z. Guo, *J. Mater. Chem. C*, 2013, **1**, 729.
53 S. Venkatraman and M. Okano, *Polym. Eng. Sci.*, 1990, **30**, 308.
54 Y. H. Wen, H. C. Lin, C. H. Li and C. C. Hua, *Polymer*, 2004, **45**, 8551.
55 Z. Guo, K. Lei, Y. Li, H. W. Ng, S. Prikhodko and H. T. Hahn, *Compos. Sci. Technol.*, 2008, **68**, 1513.
56 K. Dušek, in *Epoxy Resins and Composites III*, Springer, Berlin Heidelberg, 1986, p. 1.
57 Y. Liu, Z. Du, C. Zhang and H. Li, *Int. J. Polym. Anal. Charact.*, 2006, **11**, 299.
58 J. Jang, J. Bae and K. Lee, *Polymer*, 2005, **46**, 3677.
59 J. Stejskal, M. Trchová, J. Brodinová and I. Sapurina, *J. Appl. Polym. Sci.*, 2007, **103**, 24.
60 Y. L. Liu, *Polymer*, 2001, **42**, 3445.
61 G. Wisanrakkit, J. K. Gillham and J. B. Enns, *J. Appl. Polym. Sci.*, 1990, **41**, 1895.
62 Z. Guo, H. W. Ng, G. L. Yee and H. T. Hahn, *J. Nanosci. Nanotechnol.*, 2009, **9**, 3278.
63 T. F. Scott, W. D. Cook and J. S. Forsythe, *Eur. Polym. J.*, 2008, **44**, 3200.
64 Y. Pan, Y. Xu, L. An, H. Lu, Y. Yang, W. Chen and S. Nutt, *Macromolecules*, 2008, **41**, 9245.
65 Y. Shi, S. Peterson and D. Y. Sogah, *Chem. Mater.*, 2007, **19**, 1552.
66 Y. Sun, Z. Zhang, K.-S. Moon and C. P. Wong, *J. Polym. Sci., Part B: Polym. Phys.*, 2004, **42**, 3849.
67 T. F. Scott, W. D. Cook and J. S. Forsythe, *Polymer*, 2002, **43**, 5839.
68 X. Zhang, J. Zhu, N. Haldolaarachchige, J. Ryu, D. P. Young, S. Wei and Z. Guo, *Polymer*, 2012, **53**, 2109.
69 J. B. Enns and J. K. Gillham, *J. Appl. Polym. Sci.*, 1983, **28**, 2831.
70 B. Fabry, G. N. Maksym, J. P. Butler, M. Glogauer, D. Navajas and J. J. Fredberg, *Phys. Rev. Lett.*, 2001, **87**, 148102.
71 X. Chen, S. Wei, A. Yadav, R. Patil, J. Zhu, R. Ximenes, L. Sun and Z. Guo, *Macromol. Mater. Eng.*, 2011, **296**, 434.
72 S. R. W. E. N. Brown and N. R. Sottos, *J. Mater. Sci.*, 2004, **39**, 1703.
73 E. Sharon, S. P. Gross and J. Fineberg, *Phys. Rev. Lett.*, 1996, **76**, 2117.
74 S. Bhadra, N. K. Singha and D. Khastgir, *Curr. Appl. Phys.*, 2009, **9**, 396.
75 S. Singha and M. J. Thomas, *IEEE Trans. Dielectr. Electr. Insul.*, 2008, **15**, 12.
76 W. S. Yun, J. J. Urban, Q. Gu and H. Park, *Nano Lett.*, 2002, **2**, 447.
77 C.-D. Liu, S.-N. Lee, C.-H. Ho, J.-L. Han and K.-H. Hsieh, *J. Phys. Chem. C*, 2008, **112**, 15956.
78 A. Schonhals, H. Goering, F. R. Costa, U. Wagenknecht and G. Heinrich, *Macromolecules*, 2009, **42**, 4165.
79 F. Fang, J. Kim, H. Choi and Y. Seo, *J. Appl. Polym. Sci.*, 2007, **105**, 1853.
80 J. Lu, K.-S. Moon, B.-K. Kim and C. P. Wong, *Polymer*, 2007, **48**, 1510.